Nanoscale

High Quality Polyacrylic Acid Modified Multifunction Luminescent Nanorods for Tri-Modality Bioimaging, In Vivo Long-Lasting Tracking and Biodistribution

Journal:	*Nanoscale*
Manuscript ID:	NR-ART-09-2014-005161.R1
Article Type:	Paper
Date Submitted by the Author:	20-Oct-2014

Complete List of Authors:	Yi, Zhigao; Faculty of Material & Photoelectronic Physics, Xiangtan University lu, wei; Faculty of Applied Science and Textiles The Hong Kong Polytechnic University, Department of Applied Physics Liu, Hongrong; College of Physics and Information Science, Hunan Normal University Zeng, Songjun; College of Physics and Information Science , Hunan Normal University;

Cite this: DOI: 10.1039/c0xx00000x

www.rsc.org/xxxxxx

ARTICLE TYPE

High Quality Polyacrylic Acid Modified Multifunction Luminescent Nanorods for Tri-Modality Bioimaging, *In Vivo* Long-Lasting Tracking and Biodistribution

Zhigao Yi,[a,b] Wei Lu,[c] Hongrong Liu,[a] and Songjun Zeng [*a]

Received (in XXX, XXX) Xth XXXXXXXXX 20XX, Accepted Xth XXXXXXXXX 20XX
DOI: 10.1039/b000000x

Polyacrylic acid (PAA) modified $NaYF_4$:Gd/Yb/Er upconversion nanorods (denote as PAA-UCNRs) are demonstrated for tri-modal upconversion (UC) optical, computed X-ray tomography (CT), and magnetic resonance imaging (MRI). The hydrophilic PAA-UCNRs were obtained from hydrophobic oleic acid (OA) capped UCNRs (denote as OA-UCNRs) by using a ligand exchange method. The as-prepared UCNRs with hexagonal phase structure present high monodispersity. These PAA-UCNRs are successfully used as ideal probes for *in vivo* UC luminescent bioimaging and synergistic X-ray and UC bioimaging. Moreover, X-ray CT imaging reveals that PAA-UCNRs can act as contrast agents for improved detection of the liver and spleen. In addition, a significant signal enhancement in the liver is observed in *in vivo* MRI, indicating PAA-UCNRs are ideal T_1-weighted MRI agents. More importantly, *in vivo* long-term tracking based on these PAA-UCNRs in the live mice and corresponding *ex vivo* bioimaging of isolated organs also verify the translocation of PAA-UCNRs from the liver to spleen. And the observed intense UC signals from the feces reveal the biliary excretion mechanism of these UCNRs. These findings contribute to understanding the translocation and potential route for excretion of PAA-UCNRs, which can provide important guide for the diagnosis and detection of diseases based on these UCNRs.

1. Introduction

In recent years, bioimaging based on UC nanomaterials has attracted much research interest, which is ascribed to their unique UC emissions by large anti-Stocks shift, absence of autofluorescence, low biotoxicity in tissues, and deep penetration under near-infrared irradiation.[1-15] Among various bioimaging technologies, optical bioimaging, X-ray CT, and MRI are the most universal and widely used imaging technologies for applications in biomedicine, biolabeling, clinical diagnosis and therapy.[16-37] In comparison with traditionally optical probes such as quantum dots, organic dyes, and fluorescent probes, UC luminescent nanoprobes can not only enhance the detective sensitivity and signal-to-noise ratio but also improve the penetration depth in tissues under excitation of near-infrared light source.[38-40] In addition, lots of rare-earth (RE) compounds can also be utilized as contrast agents for CT imaging owing to large X-ray mass absorption coefficients and K-edge values of lanthanide (Ln) ions, which can provide high spatial resolution and three-dimensional (3D) information of different tissues. However, X-ray CT imaging poses intrinsic drawback of low sensitivity to soft tissues, limiting its application in disease diagnosis. MRI can afford remarkable 3D spatial and functional information of soft tissue. Combining UC optical, X-ray CT, and MRI in single system can integrate all superiorities of each single technology, which is more beneficial to diagnosis and treatment of disease. Thus, there is of significance to exploit an excellent UC nanoprobe which is suitable for simultaneous UC optical/CT/MRI bioimaging.

Among various UC nanomaterials, $NaYF_4$ has mostly used as host matrix for efficient UC emissions and optical bioimaging.[41-46] $NaYF_4$:Yb/Er nanocrystals usually possess cubic and hexagonal phase. However, as we all know, hexagonal phase $NaYF_4$ exhibits more efficient UC emissions than the cubic counterpart.[1,2] Recently, Liu's group and our previous report demonstrate that the transformation from cubic to hexagonal in $NaLnF_4$ host can be readily realized by doping Gd^{3+} at low temperature to avoid the size increase at high temperature.[27,28,47] In addition to the phase transformation induced by Gd^{3+} doping, Gd^{3+} doping can also introduce an additional X-ray imaging function owing to large k-edge value ($Gd_{k\text{-}edge}$: 50.2 keV) and high X-ray mass absorption coefficients (at 60 keV, 1.18 $cm^2\ g^{-1}$; at 80 keV, 5.57 $cm^2\ g^{-1}$).[48-50] However, there is limited reports for *in vivo* CT imaging based on $NaYF_4$:Gd/Yb/Er UCNRs. Apart from UC and X-ray absorption properties, paramagnetic property can also be improved by doping Gd^{3+} into $NaYF_4$ host due to large magnetic moment of Gd^{3+},[20,42] which makes the UCNRs ideal probes for tri-modal UC fluorescence, X-ray CT and T_1-enhanced MRI.

On the other hand, systematic study on biodistribution and metabolism of these UCNRs will provide more effective and

accurate information about physical, anatomical structure, and metabolic mechanism for clinical diagnosis and treatment.[51-54] As for $NaYF_4$:Gd/Yb/Er UCNRs, UC luminescent bioimaging is especially suitable for *in vivo* real-time tracking owing to their particularly outstanding UC emissions. However, study referred to the *in vivo* tracking and biodistribution based on $NaYF_4$:Gd/Yb/Er UCNRs is absent.

In this paper, OA-UCNRs were synthesized via a typical solvothermal method. The as-prepared hydrophobic OA-UCNRs were converted to hydrophilic PAA-UCNRs by surface ligand exchanging method using PAA as exchanging ligand. Tri-modal *in vivo* UC optical/X-ray CT/MRI based on PAA-UCNRs was demonstrated. Moreover, *in vivo* real-time and long-lasting tracking gives a glimpse to the biodistribution and excretion mechanism of PAA-UCNRs in the live mouse, which is beneficial to diagnosis and treatment in pre-clinical and clinical fields.

2. Experimental

2.1 Chemicals and Materials

RE oxides, containing Y_2O_3 (99.99%), Gd_2O_3 (99.99%), Yb_2O_3 (99.99%), and Er_2O_3 (99.99%), were purchased from Sigma-Aldrich. The corresponding nitrates $Y(NO_3)_3$, $Gd(NO_3)_3$, $Yb(NO_3)_3$, and $Er(NO_3)_3$ were obtained via adding oxides into dilute HNO_3 solution. OA, PAA (Mwt 1800), diethylene glycol (DEG), and other chemical reagents were analytically pure and obtained from Sinopharm Chemical Reagent Co., China. All reagents were used as received without purification.

2.2 Synthesis of OA-UCNRs

In a typical procedure, $NaYF_4$:Gd/Yb/Er (40:20:2 mol%) UCNRs were synthesized via a modified solvothermal process using OA as capping ligands.[27,47] At first, 1.2 g of NaOH and 2.0 mL of de-ionized (DI) water were mixed to obtain a transparent solution. And then, 10 mL of anhydrous alcohol and 20 mL of OA were added. Total amounts of $RE(NO_3)_3$ (1 mmol) with well-designed concentration and NaF (8 mmol, 1M) were added in the aforementioned solution. All procedures were carried out via agitation at room temperature. The homogeneously colloidal mixture was transferred into a 50 mL stainless Teflon-lined autoclave. The system was then heated and maintained at 170 °C for 24 h. After reaction, the system was cooled down to room temperature and products were obtained by washing with alcohol and DI water and drying at 60 °C for 6 hours.

2.3 Synthesis of PAA-UCNRs

To further application for *in vivo* bioimaging and tracking, OA-UCNRs were surface modified with PAA through ligand exchange. In a typical process,[55-57] 30 mL of DEG and 300 mg of PAA were added in a flask and heated to 110 °C with vigorously stirring under argon protection to form a clear solution. Toluene solution containing 100 mg of OA-UCNRs dispersed in cyclohexane was then injected and the system temperature maintained at 110 °C for 1 h under argon protection. After that, the system was heated to 240 °C for 1.5 h. After reaction, the system was cooled naturally and ethanol was then added to form precipitation. PAA-UCNRs were washed with DI water and ethanol several times and finally dispersed in DI water with designed concentration for further use.

2.4 Characterizations

Crystal phase of OA-UCNRs was detected by a Rigaku 2500 X-ray diffractometer utilizing a D/max-γA system at 40 kV and 250 mA with Cu-Kα radiation (λ = 1.5406 Å). Microstructures of OA-/PAA-UCNRs were characterized by FE-SEM, (FEI NanoSEM 450), TEM (JEOL-2100F), and HR-TEM. EDS (energy-dispersive X-ray spectrometer) analysis was performed under TEM assay. UC luminescent spectra were detected by a fluorescence spectrometer (Zolix fluoroSENS 9000A) equipped with a 980 nm laser. Digital photographs of the solution containing UCNRs (2 mg/mL) with different surface modification were captured using a Cannon digital camera under the 980 nm laser excitation at a power of 0.5 W.

2.5. Cytotoxicity assay

HeLa cells were cultured in Dulbecco's Modified Eagle Medium (DMEM) containing 10% fetal bovine serum, 1% penicillin and streptomycin at 37 °C and 5% CO_2. The cell toxicity of PAA-UCNRs in HeLa cells was measured via a 3-(4,5-dimethylthiazol-2-yl)-2,5 diphenyl-tetrazolium bromide (MTT) proliferation assay method. About 3×10^4 cells/well were plated in 96 well plates. After 4 h, various concentration of PAA-UCNRs (0, 25, 50, 100, 250, and 500 μg/mL) were added into the cells in the absence of serum. After 24 h of incubation, 20 μL of MTT solution was added. Blue formazan crystals were observed when checked under microscope. Media was removed and 150 μL of DMSO was added per well. The absorbance (Abs.) was measured using a microtiter plate reader. The cell viability (%) was then calculated as [Abs.490(treated cells) - background]/[Abs.490(untreated cells) -background] × 100%.

2.6 *In vivo* UC optical bioimaging

To evaluate the capability of *in vivo* UC optical bioimaging of PAA-UCNRs, a Kunming mouse was anesthetized through intraperitoneal injection with 100 μL of pentobarbital sodium aqueous solution (10 wt%). The mouse was then subcutaneously injected with 50 μL of PAA-UCNRs aqueous solution (2 mg/mL). After injection, *in vivo* UC optical bioimaging was captured using a multi-modal *in vivo* imaging system (Bruker *In-Vivo* FX PRO) under the excitation of an additional 980 nm laser as light source (Band pass filter: 535/20 nm, Exposure time: 60 s). All animal procedures comply with the institutional animal use and care regulations approved by the Laboratory Animal Center of Hunan.

2.7 *In vivo* X-ray bioimaging

To verify the capability of *in vivo* X-ray bioimaging of PAA-UCNRs, another Kunming mouse was treated through the same process and used to capture the X-ray bioimaging by the same multi-modal *in vivo* imaging system (major parameters: voltage, 45 kVp; aluminium filter, 4 mm; exposure time, 30 s).

2.8 Simultaneous *in vivo* UC optical and X-ray bioimaging

For synergistic UC optical and X-ray bioimaging based on PAA-UCNRs, a Kunming mouse was treated at first as above mentioned. Simultaneous UC optical and X-ray bioimaging were obtained via the multi-modal *in vivo* imaging system (Bruker *In-Vivo* FX PRO). The system parameters were the same as above.

2.9 *In vivo* CT imaging

In order to investigate *in vivo* CT imaging based on PAA-UCNRs, a rat was anesthetized via intraperitoneal injection with 250 μL of pentobarbital sodium aqueous solution (10 wt%). 0.8 mL of aqueous solutions containing PAA-UCNRs (20 mg/mL) were intravenously injected into the rat from tail vein. CT images were captured after 0, 30 min, and 3 h intravenous injection using a micro-CT (Hitachi Aloka Medical, Latheta LCT-200). Measurements were executed under the following parameters: base resolution, 80 × 80 μm^2; thickness, 80 μm; 80 kVp, 0.5 mA. The obtained two-dimension (2D) cross-sectional images and corresponding 3D renderings of *in vivo* CT images were analyzed with VGStudio MAX 2.2 Software.

2.10 Longitudinal relaxation time T_1, *in vitro* relaxivity measurement, and *in vivo* MRI

In vitro T_1-weighted MRI was acquired using a 1.2 T Magnetom system (HT-ANNMR-50, Shanghai Shinning Global Scientific and Educational Equipment Co.). Aqueous solutions containing PAA-UCNRs with well-designed Gd^{3+} concentrations at 0, 0.0625, 0.125, 0.25, 0.5, 1.0, and 2.0 mg/mL were transferred into 1.0 mL tubes for T_1-weighted MRI. T_1-weighted sequence was performed as follows: Spin Echo (SE), TR = 100 ms, TE = 9.6 ms, matrix = 256 × 256, FOV = 50 × 130, slice thickness = 1.5 mm. Relaxivity values were calculated using the linear fitting of $1/T_1$ relaxation time as a function of Gd^{3+} concentrations.

For further *in vivo* MRI, a Kunming mouse after intraperitoneal injection of pentobarbital sodium aqueous solution was intravenously injected with 50 μL of PAA-UCNRs aqueous solution (2 mM Gd^{3+} concentration). *In vivo* MRI was also performed by a 1.2 T Magnetom system (HT-ANNMR-50, Shanghai Shinning Global Scientific and Educational Equipment Co.) using a T_1-weighted sequence: Spin Echo (SE), TR = 100 ms, TE = 9.6 ms, Flip angle = 120, FOV = 50 × 130, matrix = 256 × 256, slice thickness = 1.5 mm. Coronal cross-sectional images of the mouse were captured before and after 30 min intravenous injection.

2.11 *In vivo* real-time tracking

For further investigation on biodistribution of PAA-UCNRs, groups of Kunming mice were first anesthetized by intraperitoneal injection of pentobarbital sodium aqueous solution (100 μL, 10 wt%) and then injected 100 μL of PAA-UCNRs solution (2 mg/mL) from tail vein. Bright field images and *in vivo* UC luminescent bioimaging at different time intervals were captured under the multi-modal *in vivo* imaging system. The feces of a mouse was collected after 12 h injection and used for UC signal detection.

And then, Kunming mice with intravenous administration of PAA-UCNRs were scarified at designed time points. After dissection, the various organs of the sacrificed mice including heart, lung, liver, spleen, and kidney were used for detecting bright field images and UC luminescent signal via the multi-modal *in vivo* imaging system.

3. Results and Discussion

3.1 Phase and microstructure of OA-/PAA-UCNRs

As illustrated in Scheme 1, PAA-UCNRs were obtained by ligand exchange from OA-UCNRs prepared via a typical solvothermal method. PAA-UCNRs were further served as bio-probes and contrast agents for tri-modal *in vivo* UC optical/X-ray CT/MRI imaging and real-time UC luminescence tracking.

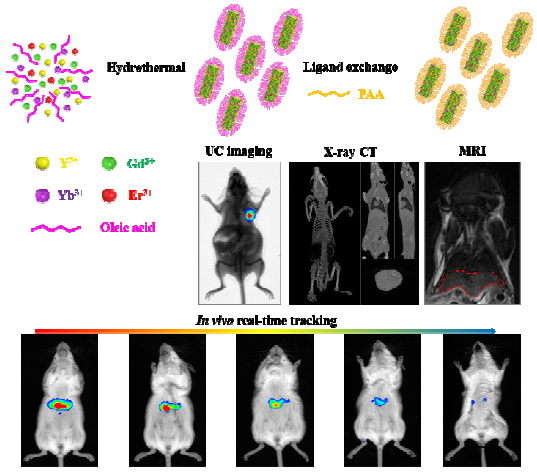

Scheme 1. Schematic illustration of the synthesis process of PAA-UCNRs, application for tri-modal *in vivo* UC optical/X-ray CT/MRI imaging and biodistribution.

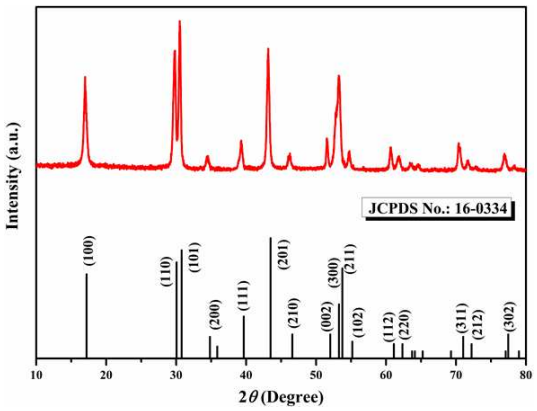

Figure 1. XRD pattern of OA-UCNRs (red curve) and standard hexagonal phase $NaYF_4$ data (JCPDS FILE No. 16-0334).

Crystal phase and phase compositions of OA-UCNRs were analyzed by X-ray powder diffraction (XRD) pattern. As shown in Figure 1, all of the diffraction peaks of XRD patterns were well indexed as pure hexagonal phase $NaYF_4$ (JCPDS FILE No. 16-0334). Diffraction peaks shifted toward lower diffraction angles implying the increase of the unit-cell volume, which is ascribed to substitution of Y^{3+} by larger ionic radii of Gd^{3+} and Yb^{3+}.[58] In addition, the diffraction peaks of Gd-free UCNRs (Figure S1) were also indexed with the standard hexagonal phase $NaYF_4$ (JCPDS FILE No. 16-0334), indicating that the crystal phase is maintained after doping Gd^{3+}. This is mainly ascribed to the high synthesis temperature and long reaction time for Gd-free sample, which is beneficial to form hexagonal phase structure.

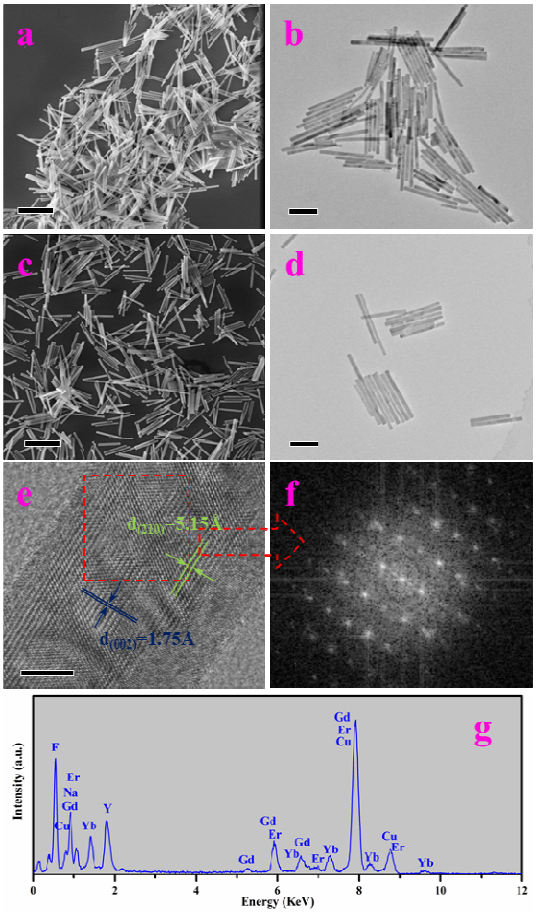

Figure 2. Microstructures study of OA-/PAA-UCNRs. FE-SEM of (a) OA-UCNRs, (c) PAA-UCNRs; TEM images of (b) OA-UCNRs, (d) PAA-UCNRs; (e) HR-TEM of a single nanorod from (d), (f) corresponding FFT of HR-TEM; and (g) EDS of OA-UCNRs. Scale bars are 200 nm for a-d and 10 nm for f.

Morphology and size of OA-/PAA-UCNRs were characterized by FE-SEM (Figure 2a and 2c) and TEM (Figure 2b and 2d) assays. As shown in FE-SEM and TEM images, OA-UCNRs present rod-like shape with high monodispersity. After surface modification with PAA, morphology of these UCNRs is still maintained. Moreover, PAA-UCNRs (Figure 2c and 2d) are highly monodispersed. The mean length and diameter based on TEM image of OA-UCNRs were about 327 and 25 nm, respectively. However, the average length and diameter of Gd-free UCNRs based on TEM images (Figure S2) were measured to be 1790 and 84 nm, respectively. In comparison with Gd-free UCNRs, the length and diameter of UCNRs were dramatically decreased after doping 40% Gd^{3+}. To further investigate the diepersibility, the size distribution of PAA-UCNRs in aqueous solution and phosphate buffer solution (pH = 7.4) was measured by DLS (Figure S3). The DLS results inveal that PAA-UCNRs present monodispersity in the both solutions. HR-TEM image (Figure 2e) of a single nanorod from Figure 2d and the corresponding Fast Fourier Transform image (FFT, Figure 2f) show that the single nanorod possesses single-crystalline nature. The interplanar distances were measured to be about 1.75 and 5.15 Å, corresponding to the (002) and (210) lattice planes of hexagonal phase, respectively, which matched well with the aforementioned XRD analysis. In addition, the preferred growth direction of OA-UCNRs is along the [001] direction. The detected element compositions of OA-UCNRs (Figure 2g) reveal that the main elemental components are Na, Y, F, Gd, Yb, and Er. Notably, the detected Cu element comes from Cu grid of TEM.

3.2 UC luminescent properties of OA-/PAA-UCNRs

UC luminescent properties of OA-/PAA-UCNRs were studied from the emission spectra. As shown in Figure S4, the two intense green emissions are ascribed to the transitions $^2H_{11/2} \rightarrow {}^4I_{15/2}$ and $^4S_{3/2} \rightarrow {}^4I1_{5/2}$, which accordant with the green emissions in Figure 3a peaked on 520 and 540 nm, respectively. In addition, the red emission is attributed to the transition $^4F_{9/2} \rightarrow {}^4I_{15/2}$, matching with the red emission centered at 660 nm. The emission intensity of PAA-UCNRs (Figure 3a) was only slightly lower than OA-capped one. Digital photographs present intense eye-visible green light of both OA-UCNRs (Figure 3b) and PAA-UCNRs (Figure 3c) under the 980 nm laser excitation at a low power of 0.5 W.

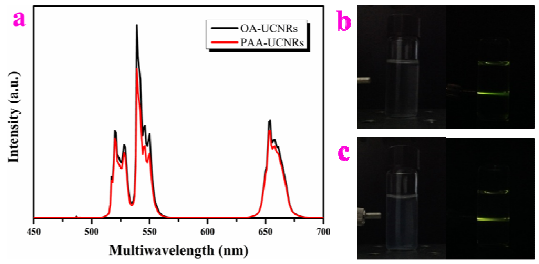

Figure 3. UC luminescence properties of OA-/PAA-UCNRs. (a) UC emission spectra and digital photographs based on (b) OA-UCNRs in cyclohexane solution and (c) PAA-UCNRs in aqueous solution, respectively.

3.3 Cell toxicity test

Low cell toxicity of nanoprobes is required for the biomedical application. To evaluate the cytotoxicity and biocompatibility of PAA-UCNRs, cell viability of PAA-UCNRs in HeLa cells was measured via a MTT method. As demonstrated in Figure 4, cell viability was above 90% when treated with 0-250 μg/mL PAA-UCNRs for 24 h. When the concentration of PAA-UCNRs was increased up to 500 μg/mL, the cellular viability is estimated to be 86%, indicating that remarkable low cytotoxicity of PAA-UCNRs. Therefore, PAA-UCNRs can be used as ideal bioprobes with very low cytotoxicity.

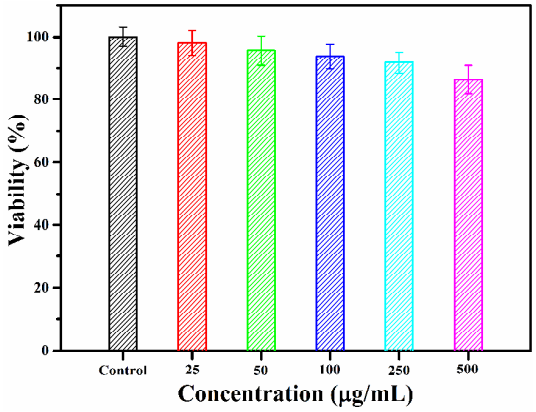

Figure 4. MTT assay for cell toxicity of PAA-UCNRs in HeLa cells treated with different concentrations of PAA-UCNRs at 37 °C for 24 h under 5% CO_2.

3.4 *In vivo* UC luminescent/X-ray bioimaging and synergistic UC optical/X-ray bioimaging

To verify the feasibility of PAA-UCNRs for *in vivo* UC luminescent imaging, a Kunming mouse was subcutaneously injected with 50 μL of aqueous solution containing PAA-UCNRs (2 mg/mL) and UC signal was captured under the 980 nm laser excitation. As presented in Figure 5b, intense UC signal can be detected from the treated mouse, while no luminescent signal was observed before injection (Figure 5a). It implies that PAA-UCNRs are promising nanoprobes for UC luminescent imaging. Owing to large X-ray mass attenuation coefficients and K-edge values of the highly doped Gd^{3+}, PAA-UCNRs also exhibit their well absorption properties for *in vivo* X-ray bioimaging. As shown in Figure S5, another Kunming mouse was subcutaneously injected with 50 μL of aforementioned solution containing PAA-UCNRs. In comparison to the untreated mouse (Figure S5a), the mouse after injection shows high contrast in the injected location (red arrow shown in Figure S5b). The results indicate that PAA-UCNRs can also be used as ideal contrast agents for *in vivo* X-ray imaging.

To further study the feasibility of *in vivo* synergistic dual-modal imaging, the mouse before and after treatment were performed using a multi-modal *in vivo* bioimaging system. As demonstrated in the left panel of Figure 5d, the treated mouse shows obvious X-ray contrast in the injection location while comparing with the one before injection (Figure 5c). Besides, intense UC signal was captured in the same injection region (middle panel of Figure 5d), which matches well with X-ray contrast (right panel of Figure 5d), indicating the realization of simultaneous *in vivo* X-ray and UC luminescence bioimaging in the same location by intergrating the two imaging modalities.

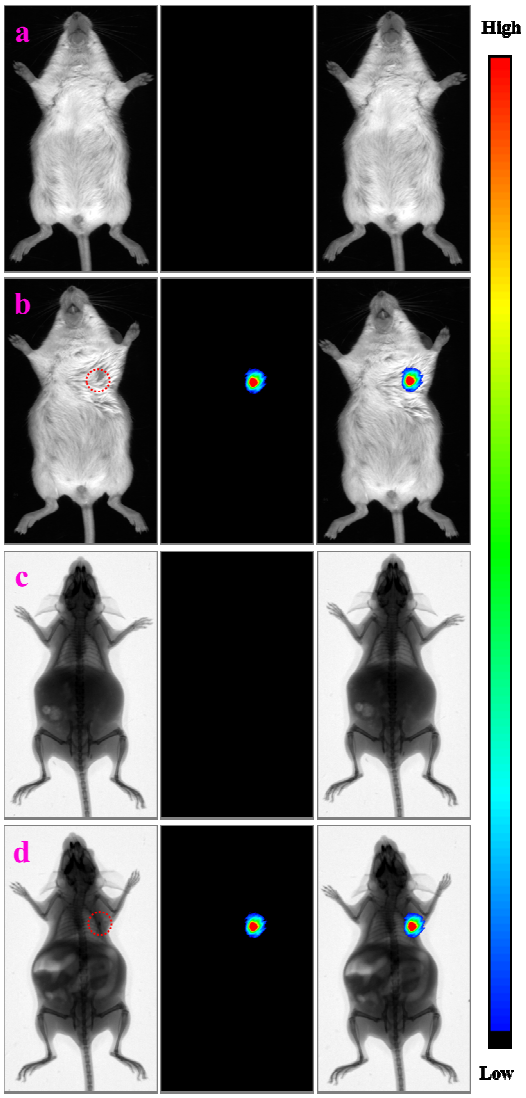

Figure 5. *In vivo* UC luminescent of a Kunming mouse: (a) without and (b) with subcutaneous injection of PAA-UCNRs. Synergistic *in vivo* UC luminescent and X-ray bioimaging: (c) without and (d) with subcutaneous injection of PAA-UCNRs. The panels ranging from left to right are bright field/X-ray, UC, and overlay images, respectively.

3.5 *In vivo* X-ray CT imaging

High X-ray absorption coefficients of Gd^{3+} in PAA-UCNRs inspire us to pursue *in vivo* X-ray CT imaging based on PAA-UCNRs. To further validate the whole-body CT imaging based on these PAA-UCNRs, a rat intravenously administered aqueous solution containing PAA-UCNRs (0.8 mL, 20 mg/mL) was detected by X-ray micro-CT imaging at different time points. As illustrated in Figure 6a, no signal of soft tissues was detected from the untreated rat. After 30 min intravenous injection, dominant signal in the liver location and weak signal from the spleen region can be observed from 3D volume-rendered CT image (left and middle panels of Figure 6b) and the maximum intensity projection from cross section of various directions (right panel of Figure 6b). As shown in Figure 6c, significant enhancement of signal in the liver and spleen regions was observed after 3 h injection. Moreover, some signal can be

observed in intestines sites after injection (Figure 6b and 6c), indicating that the main metabolic pathway of these PAA-UCNRs is biliary excretion mechanism for these nanoparticles to the intestine and finally excretion with the feces, which coincides with later *in vivo* UC luminescent tracking analysis. This excretion route is different from the previous reported renal excretion pathway based on the ultra-small nanoparticles.[32] The perfect X-ray attenuation property of PAA-UCNRs makes them ideal contrast agents for X-ray CT imaging.

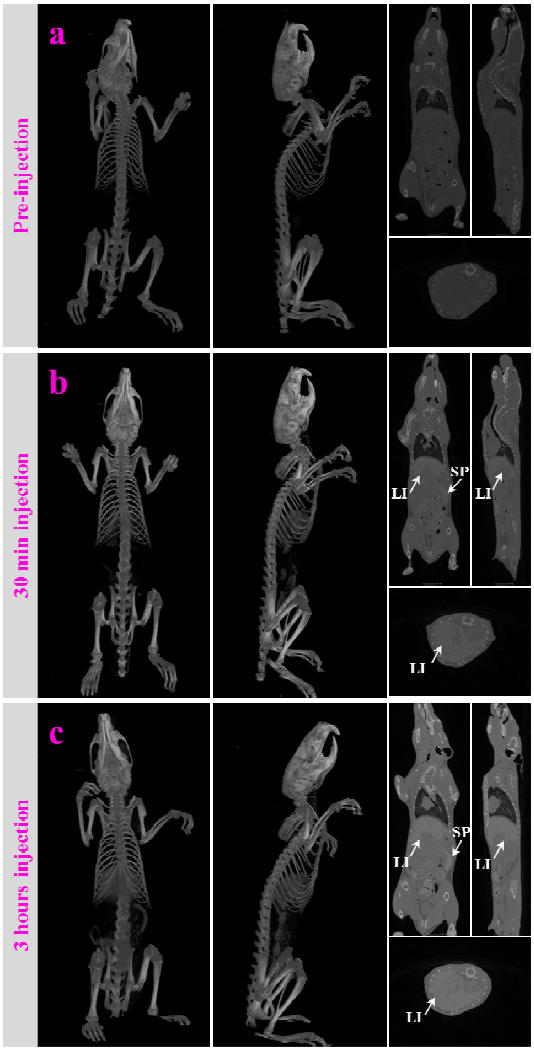

Figure 6. *In vivo* X-ray CT imaging of a rat before and after intravenous injection from tail vein with 0.8 mL of PAA-UCNRs (20 mg/mL) at different time intervals: (a) pre-injection, (b) 30 min, and (c) 3 h. The left and middle panels are the 3D volume-rendered *in vivo* CT images from the top and lateral view. The right panel is the maximum intensity projection of the rat which contains coronal, sagittal, and transversal planes, where the regions with high contrast after treatment were marked (LI: liver, SP: spleen).

3.6 *In vitro* T_1-weighted and *in vivo* MRI

To evaluate MRI feasibility of PAA-UCNRs, *in vitro* T_1-weighted relaxivity measurement was conducted on a 1.2 T Magnetom system. A series of tubes containing the water solutions with well-designed Gd^{3+} concentrations were arrayed in sequence. As demonstrated in Figure 7a, a positive enhancement of MRI signal was detected when increasing Gd^{3+} concentration. Besides, the T_1 relaxivity coefficients of PAA-UCNRs were measured at the same time. Figure 7b shows the $1/T_1$ values as a function of Gd^{3+} concentration. The r_1 value of PAA-UCNRs was linearly fitted and calculated to be 3.36 $mM^{-1}s^{-1}$.

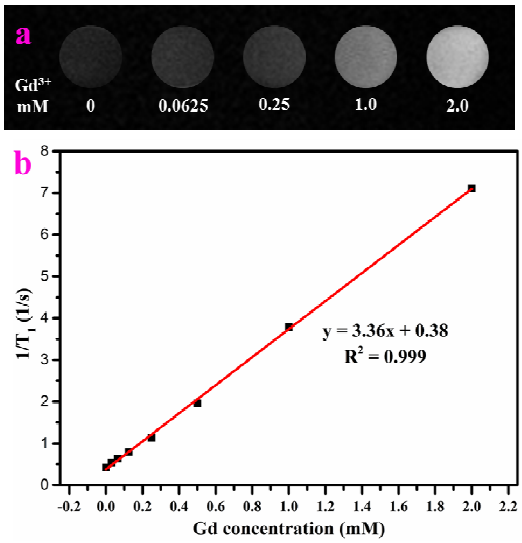

Figure 7. (a) *In vitro* T_1-weighted MRI images of PAA-UCNRs dissolved in water with well-designed concentrations, (b) relaxation rate r_1 ($1/T_1$) versus molar concentrations of aqueous suspension of PAA-UCNRs.

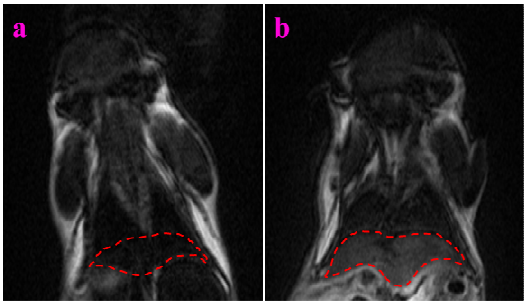

Figure 8. *In vivo* MRI coronal images of a Kunming mouse (a) before and (b) after 30 min intravenous injection from tail vein with 50 μL of PAA-UCNRs (2 mM Gd^{3+} concentration).

To further examine the performance of PAA-UCNRs for MRI, *in vivo* MRI was also demonstrated by a Kunming mouse after intravenous injection from tail vein with 50 μL of PAA-UCNRs (2 mM Gd^{3+} concentration). As shown in Figure 8b, significant positive-contrast enhancement is observed in the liver region (red-dotted region in Figure 8) after 30 min treatment. However, there was no obvious contrast signal in the same location before injection (Figure 8a). *In vitro* T_1 relaxivity measurement and *in vivo* MRI results indicate that PAA-UCNRs could be used as ideal MRI contrast agents.

3.7 *In vivo* real-time biodistribution and long-term tracking

Long-term translocation and clearance of bio-probes in the live animals provide a reference of the interaction mechanism between biotissues and nanoprobes. Therefore, groups of

Kunming mice intravenously injected with PAA-UCNRs were used for *in vivo* and *ex vivo* UC luminescent bioimaging. As shown in Figure 9a, intense UC signal was detected in the liver location after 15 min treatment and gradually decreased with increasing injection time. Translocation of PAA-UCNRs in the live mouse was further revealed by average intensity of UC signal. As illustrated in Figure 9c, UC signal was gradually decreased in the liver location with prolonging the injection time. Further *ex vivo* UC luminescent bioimaging of various organs (Figure 9b) shows the same changing trend in the liver location. After 96 h injection, a significant UC signal can still be observed. As observed from Figure 9b, there was always limited UC signal remained in the lung region after injection, indicating that a small amount of PAA-UCNRs aggregated in the lungs and extended period are needed for clearance of PAA-UCNRs. The statistical average values of various isolated organs at different time points (Figure 9d) accurately reveal that UC signal decreases sharply in the liver region and reduces gradually in the lungs as a function of injection time. Weak UC signal can be observed in the spleen site from the isolated organs (Figure 9b) after 12 h injection, implying translocation of PAA-UCNRs from the liver to spleen. To further verify the excretion mechanism of PAA-UCNRs, the feces of the mouse after 12 h injection were collected for UC signal detection. As shown in Figure 9e, intense UC signals are detected from the feces, unambiguously validating that the clearance mechanism of PAA-UCNRs is actually hepatobiliary excretion, which coincides with the former X-ray CT imaging result. These findings reveal that PAA-UCNRs are mainly accumulated in liver at initial injection time, which is different from the results reported by Liu's group and our previous work based on UC nanoparticles with relatively small size, in which nanoprobes were initially assembled in the lungs and then transferred to the liver.[33,34] Obviously, size and shape of UC nanoprobes have a great effect on their biodistribution and excretion mechanism in the live animals, which needs further systematic study. The long-term *in vivo* tracking and biodistribution analysis indicate that PAA-UCNRs are perfect UC optical nanoprobes and can provide clues on the fundamental study of pharmacy and further application in diagnosis and therapy.

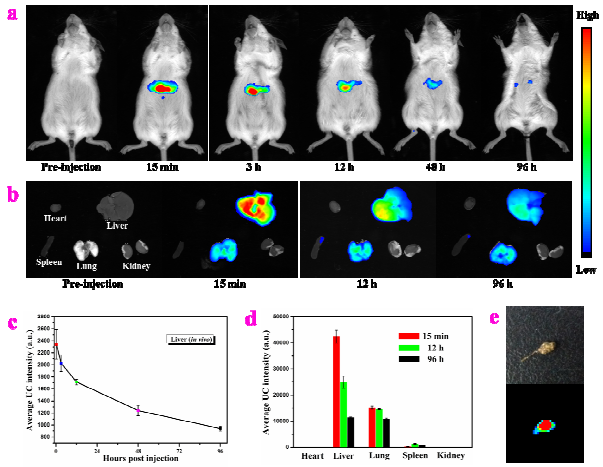

Figure 9. *In vivo* tracking and long-term biodistribution of PAA-UCNRs: (a) *In vivo* UC imaging, (b) the corresponding images of the isolated organs (including heart, liver, spleen, lung, and kidney) at different time points, (c) time-dependent average intensity of UC optical signals taken from liver areas in the live mice, (d) intensity distribution in different organs and (e) digital photograph and UC imaging of the feces collected from the live mouse after 12 h injection. Error bars for c and d were based on three mice per group.

4. Conclusion

In this paper, PAA-UCNRs through ligand exchange method present pure hexagonal phase and outstanding UC luminescence. Simultaneous *in vivo* UC optical and X-ray bioimaging indicates the multifunctional bioimaging feasibility of PAA-UCNRs. X-ray CT imaging shows the high contrast effect in the liver and spleen regions and potential hepatobiliary excretion of PAA-UCNRs. *In vivo* T_1-weighted MRI reveals that PAA-UCNRs can emerge as positive contrast MRI agents. Moreover, *in vivo* long-term tracking and real-time biodistribution based on PAA-UCNRs in the live mice provide more sufficient evidence on translocation and hepatobiliary excretion mechanism of PAA-UCNRs. *In vivo* tri-modal UC optical/X-ray CT/MRI imaging and long-lasting tracking capability in the live mice make PAA-UCNRs ideal bio-probes for applications in biological and clinical fields.

Acknowledgments

This work was supported by the National Natural Science Foundation of China (Nos. 51102202, and 31370736), Specialized Research Fund for the Doctoral Program of Higher Education of China (No. 20114301120006) and Hunan Provincial Natural Science Foundation of China (No. 12JJ4056), and Scientific Research Fund of Hunan Provincial Education Department (13B062).

Notes and references

[a] *College of Physics and Information Science and Key Laboratory of Low-dimensional Quantum Structures and Quantum Control of the Ministry of Education, Hunan Normal University, Changsha 410081, Hunan, China. Email: songjunz@hunnu.edu.cn*

[b] *School of Materials Science and Engineering, Key Laboratory of Low-dimensional Materials and Application Technology (Ministry of Education), Xiangtan University, Xiangtan 411105, China.*

[c] *Materials Research Center and Department of Applied Physics, The Hong Kong Polytechnic University, Hong Kong.*

1. J. W. Card, D. C. Zeldin, J. C. Bonner and E. R. Nestmann, *Am. J. Physiol. Lung Cell Mol. Physiol.*, 2008, **295**, L400.
2. M. E. Akerman, W. C. Chan, P. Laakkonen, S. N. Bhatia and E. Ruoslahti, *Proc. Natl. Acad. Sci. USA*, 2002, **99**, 12617.
3. R. A. Tripp, R. Alvarez, B. Anderson, L. Jones, C. Weeks and W. Chen, *Int. J. Nanomed.*, 2007, **2**, 117.
4. E. B. Voura, J. K. Jaiswal, H. Mattoussi and S. M. Simon, *Nat. Med.*, 2004, **10**, 993.
5. J. Zhou, Z. Liu and F. Y. Li, *Chem. Soc. Rev.*, 2012, **41**, 1323.
6. M. Haase and H. Schäfer, *Angew. Chem. Int. Ed.*, 2011, **50**, 5808.
7. F. Wang, R. R. Deng, J. Wang, Q. X. Wang, Y. Han, H. M. Zhu, X. Y. Chen and X. G. Liu, *Nat. Mater.*, 2011, **10**, 968.
8. H. Mader, P. Kele, S. Saleh and O. Wolfbeis, *Curr. Opin. Chem. Biol.*, 2010, **14**, 582.
9. G. Y. Chen, T. Y. Ohulchanskyy, R. Kumar, H. Ågren and P. N. Prasad, *ACS Nano*, 2010, **4**, 3163.

10. Y. S. Liu, D. T. Tu, H. M. Zhu and X. Y. Chen, *Chem. Soc. Rev.*, 2013, **42**, 6924.
11. J. C. Boyer and F. C. J. M. van Veggel, *Nanoscale*, 2010, **2**, 1417.
12. S. J. Zeng, Z. G. Yi, W. Lu, C. Qian, H. B. Wang, L. Rao, T. M. Zeng, H. R. Liu, H. J. Liu, B. Fei and J. H. Hao, *Adv. Func. Mater.*, 2014, **24**, 4196.
13. S. Hilderbrand and R. Weissleder, *Curr. Opin. Chem. Biol.*, 2010, **14**, 71.
14. T. Jamieson, R. Bakhshi, D. Petrova, R. Pocock, M. Imani and A. M. Seifalian, *Biomaterials*, 2007, **28**, 4717.
15. N. M. Idris, M. K. Gnanasammandhan, J. Zhang, P. C. Ho, R. Mahendran and Y. Zhang, *Nat. Med.*, 2012, **18**, 1580.
16. M. Nyk, R. Kumar, T. Y. Ohulchanskyy, E. J. Bergey and P. N. Prasad, *Nano Lett.*, 2008, **8**, 3834.
17. S. J. Zeng, M. K. Tsang, C. F. Chan, K. L. Wong and J. H. Hao, *Biomaterials*, 2012, **33**, 9232.
18. L. Q. Xiong, T. S. Yang, Y. Yang, C. J. Xu and F. Y. Li, *Biomaterials*, 2010, **31**, 7078.
19. S. J. Zeng, M. K. Tsang, C. F. Chan, K. L. Wong, B. Fei and J. H. Hao, *Nanoscale*, 2012, **4**, 5118.
20. D. K. Chatteriee, A. J. Rufalhah and Y. Zhang, *Biomaterials*, 2008, **29**, 937.
21. J. Wang, F. Wang, C. Wang, Z. Liu and X. G. Liu, *Angew. Chem. Int. Ed.*, 2011, **50**, 10369.
22. C. Wang, H. Q. Tao, L. Cheng and Z. Liu, *Biomaterials*, 2011, **32**, 6145.
23. L. Cheng, K. Yang, Y. G. Li, J. H. Chen, C. Wang, M. W. Shao, S. T. Lee and Z. Liu, *Angew. Chem. Int. Ed.*, 2011, **50**, 7385.
24. W. P. Fan, B. Shen, W. B. Bu, F. Chen, K. L. Zhao, S. J. Zhang, L. P. Zhou, W. J. Peng, Q. F. Xiao, H. Y. Xing, J. N. Liu, D. L. Ni, Q. J. He and J. L. Shi, *J. Am. Chem. Soc.*, 2013, **135**, 6494.
25. Q. F. Xiao, X. P. Zheng, W. B. Bu, W. Q. Ge, S. J. Zhang, F. Chen, H. Y. Xing, Q. G. Ren, W. P. Fan, K. L. Zhao, Y. Q. Hua and J. L. Shi, *J. Am. Chem. Soc.*, 2013, **135**, 13041.
26. Y. L. Liu, K. L. Ai, J. H. Liu, Q. H. Yuan, Y. Y. He and L. H. Lu, *Angew. Chem. Int. Ed.*, 2012, **51**, 1437.
27. S. J. Zeng, J. J. Xiao, Q. B. Yang and J. H. Hao, *J. Mater. Chem.*, 2012, **22**, 9870.
28. S. J. Zeng, H. B. Wang, W. Lu, Z. G. Yi, L. Rao, H. R. Liu and J. H. Hao, *Biomaterials*, 2014, **35**, 2934.
29. Z. G. Yi, S. J. Zeng, W. Lu, H. B. Wang, L. Rao, H. R. Liu and J. H. Hao, *ACS Appl. Mater. Interfaces*, 2014, **6**, 3839.
30. Y. Sun, J. J. Peng, W. Feng and F. Y. Li, *Theranostics*, 2013, **3**, 346.
31. X. J. Zhu, J. Zhou, M. Chen, M. Shi, W. Feng and F. Y. Li, *Biomaterials*, 2012, **33**, 4618.
32. T. Y. Cao, Y. Yang, Y. Sun, Y. Q. Wu, Y. Gao, W. Feng and F. Y. Li, *Biomaterials*, 2013, **34**, 7127.
33. C. Wang, L. Cheng, H. Xu and Z. Liu, *Biomaterials*, 2012, **33**, 4872.
34. Z. G. Yi, W. Lu, Y. R. Xu, J. Yang, L. Deng, C. Qian, T. M. Zeng, H. B. Wang, L. Rao, H. R. Liu and S. J. Zeng,. *Biomaterials*, 2014, DIO: 10.1016/j.biomaterials.2014.08.021.
35. A. Jakhmola, N. Anton and T. F. Vandamme, *Adv. Healthc. Mater.*, 2012, **1**, 413.
36. D. Pan, E. Roessl, J. P. Schlomka, S. D. Caruthers, A. Senpan, M. J. Scott, J. S. Allen, H. Y. Zhang, G. Hu, P. J. Gaffney, E. T. Choi, V. Rasche, S. A. Wickline, R. Proksa and G. M. Lanza, *Angew. Chem. Int. Ed.*, 2010, **49**, 9635.
37. Y. L. Liu, K. L. Ai, J. H. Liu, Q. H. Yuan, Y. Y. He and L. H. Lu, *Adv. Healthc. Mater.*, 2012, **1**, 461.
38. M. Beija, C. A. M. Afonso and J. M. G. Martinho, *Chem. Soc. Rev.*, 2009, **38**, 2410.
39. B. N. Giepmans, S. R. Adams, M. H. Ellisman and R. Y. Tsien, *Science*, 2006, **312**, 217.
40. Q. B. Wang, Y. Liu, Y. G. Ke and H. Yan, *Angew. Chem. Int. Ed.*, 2008, **47**, 316.
41. Z. L. Wang, J. H. Hao, H. L. W. Chan, W. T. Wong and K. L. Wong, *Small*, 2012, **8**, 1863.
42. J. Zhou, M. X. Yu, Y. Sun, X. Z. Zhang, X. J. Zhu, Z. H. Wu, D. M. Wu and F. Y. Li, *Biomaterials*, 2011, **32**, 1148.
43. X. F. Yu, M. Li, M. Y. Xie, L. D. Chen, Y. Li and Q. Q. Wang, *Nano Res.*, 2010, **3**, 51.
44. G. Y. Chen, T. Y. Ohulchanskyy, R. Kumar, H. Ågren and P. N. Prasad, *ACS Nano*, 2010, **4**, 3163.
45. J. C. Boyer, F. Vetrone, L. A. Cuccia and J. A. Capobianco, *J. Am. Chem. Soc.*, 2006, **128**, 7444.
46. M. Wang, C. C. Mi, W. X. Wang, C. H. Liu, Y. F. Wu, Z. R. Xu, C. B. Mao and S. K. Xu, *ACS Nano*, 2009, **3**, 1580.
47. F. Wang, Y. Han, C. S. Lim, Y. H. Lu, J. Wang, J. Xu, H. Y. Chen, C. Zhang, M. H. Hong and X. G. Liu, *Nature*, 2010, **463**, 1061.
48. S. B. Yu and A. D. Watson, *Chem. Rev.*, 1999, **99**, 2353.
49. http://physics.nist.gov/PhysRefData/XrayMassCoef/
50. Z. Liu, F. Pu, S. Huang, Q. H. Yuan, J. S. Ren and X. G. Qu, *Biomaterials*, 2013, **34**, 1712.
51. L. Cheng, K. Yang, M. Shao, X. Lu and Z. Liu, *Nanomedicine*, 2011, **6**, 1327.
52. Y. Yang, Y. Sun, T. Y. Cao, J. J. Peng, Y. Liu, Y. Q. Wu, W. Feng, Y. J. Zhang and F. Y. Li, *Biomaterials*, 2013, **34**, 774.
53. R. A. Jalil and Y. Zhang, *Biomaterials*, 2008, **29**, 4122.
54. L. Xiong, T. S. Yang, Y. Yang, C. J. Xu and F. Y. Li, *Biomaterials*, 2010, **31**, 7078.
55. T. R. Zhang, J. P. Ge, Y. X. Hu and Y. D. Yin, *Nano Lett.*, 2007, **7**, 3203.
56. R. Naccache, F. Vetrone, V. Mahalingam, L. A. Cuccia and J. A. Capobianco, *Chem. Mater.*, 2009, **21**, 717.
57. T. S. Yang, Y. Sun, Q. Liu, W. Feng, P. Y. Yang and F. Y. Li, *Biomaterials*, 2012, **33**, 3733.
58. R. D. Shannon, *Acta Cryst.*, 1976, **A32**, 751.